Review

CONTRAST MEDIA & MOLECULAR IMAGING

Received: 2 December 2010, Revised: 7 February 2011, Accepted: 11 February 2011, Published online in Wiley Online Library: 2011

(wileyonlinelibrary.com) DOI: 10.1002/cmmi.442

Multifunctional microbubbles and nanobubbles for photoacoustic imaging†

Ronald X. Xu[a]*

Photoacoustic imaging is an emerging imaging modality for noninvasive detection of tissue structural and functional anomalies. Multifunctional microbubbles (MBs) and nanobubbles (NBs) are contrast agents integrating multiple disease-targeting, imaging and therapeutic functions. Multifunctional MBs and NBs represent an enabling technology for many potential applications in the field of photoacoustic imaging. Highly absorbing optical contrast agents, such as gold nanoparticles, India ink and Indocyanine Green, can be encapsulated in MBs and NBs for stable absorption properties and multimodal imaging contrasts. The surface of MBs and NBs can be modified for high disease-targeting affinity, reduced immunogenicity and prolonged circulation lifetime. Low boiling point perfluorocarbon compounds can be encapsulated in MBs and NBs for selective activation by external energy sources. The activation of these MBs and NBs may introduce significant contrast enhancement and facilitate a variety of potential clinical applications, such as image-guided drug delivery and therapeutic margin assessment. MB and NB enhanced photoacoustic imaging is still in its infancy. Further development and validation works are necessary for successful translation of the technology from the benchtop to the bedside. Copyright © 2011 John Wiley & Sons, Ltd.

Keywords: microbubble; nanobubble; nanocapsule; nanoballoon; photoacoustic imaging; ultrasonography; fluorescence; multimodal imaging; conjugation; drug delivery

1. INTRODUCTION

Ultrasonography (US) is a low-cost and portable imaging modality commonly used in clinical diagnosis and image-guided intervention (1). Gas-filled microbubbles (MBs) have been used for contrast enhancement in US imaging. Presently, MBs are approved in Europe, Asia and Canada, while the Food and Drug Administration (FDA) in the USA has not yet approved MBs for noncardiac use (2). MBs are commonly considered as blood-pool contrast agents. They can be delivered intravenously and safely circulate in the human vascular system for contrast enhanced US imaging of tissue structural and functional anomalies (3). The emergence of target-specific and drug-loaded MBs has opened a new avenue for molecular US imaging and image-guided therapy (4–6). In addition to MBs, various nanoparticles, including nanobubbles (NBs) with diameters around several hundred nanometers, have also been explored for targeted imaging and therapeutic applications (7,8). NBs also demonstrate the enhanced contrast in US imaging, possibly due to particle aggregation, coalescence and layering effects (7,9). The emergence of multifunctional MB and NB agents has empowered the traditional US imaging with new capabilities for integrated diagnosis and image-guided therapy.

Photoacoustic imaging is an emerging imaging modality that integrates the molecular sensitivity of optical imaging and the spatial resolution of US imaging (10). Photoacoustic imaging detects functional properties of subcutaneous tissue structures in a cross-sectional area or a three-dimensional space based on the photoacoustic effect (11). A photoacoustic imaging system uses a short-pulse light beam to illuminate biological tissue and excite tissue chromophores for thermoelastic expansion. The resultant pressure wave propagation is captured by an ultrasonic transducer. The spatial concentration of tissue chromophores is then obtained by either point-to-point scanning (for a scanning focused US detector or a scanning focused illuminating laser beam) (12–14) or inverse image reconstruction (for an array of unfocused ultrasonic transducers) (15). Owing to its high sensitivity to optical absorption, photoacoustic imaging has been used to detect both endogenous and exogenous chromophores. Endogenous chromophores include oxygenated and deoxygenated hemoglobin (16). Exogenous chromophores include Indocyanine green (ICG) (17), methylene blue (18) and gold nanoparticles (19–21).

MBs and NBs have the potential to play an important role in photoacoustic imaging. Previous reports have demonstrated the technical feasibility of MB- and NB-enhanced photoacoustic imaging (22,23). However, this research field is still in its infancy. Therefore, a comprehensive review is not possible. This paper aims at introducing the MB and NB agents, explaining their fabrication processes, highlighting their potential applications in photoacoustic imaging, addressing technical opportunities and challenges, and discussing future perspectives. It is the author's hope that the paper will stimulate broad research interests in this emerging research field of great promise.

* *Correspondence to: R. Xu, Department of Biomedical Engineering, The Ohio State University, 270 Bevis Hall, 1080 Carmack Rd, Columbus, OH 43210, USA. E-mail: xu.202@osu.edu*

a *R. X. Xu*
Department of Biomedical Engineering, The Ohio State University, 270 Bevis Hall, 1080 Carmack Rd, Columbus, OH 43210, USA

† *This article is published in Contrast Media and Molecular Imaging as part of the special issue on Photoacoustic Imaging, edited by Dr. Gregory Lanza, Department of Medicine, Washington University Medical Hospital.*

Biography

Dr Ronald X. Xu, earned his Ph.D. in Mechanical Engineering from Massachusetts Institute of Technology. His primary research interest is to develop handheld imaging tools and biodegradable contrast agents for cancer detection, intraoperative imaging and image-guided therapy. He has been Principal Investigator (or Co-investigator) of over five clinical trials at the Ohio State University Medical Center. He is also inventor (or co-inventor) of eight published patents. In 2010, he was profiled as one of the 10 'Superstars' by the *Columbus CEO Magazine*. In 2011, he was awarded the TechColumbus 'Inventor of the Year'.

2. MICROBUBBLES, NANOBUBBLES AND THEIR FABRICATION PROCESSES

MBs in general are gas bubbles with diameters ranging from 1 to 1000 μm (24). MBs for *in vivo* imaging and therapeutic applications typically have diameters from 2 to 6 μm to assure successful circulation in the human vascular system. Many MB agents, such as Albunex, Echovist, Levovist, EchoGen, Optison, Definity and SonoVue, have been approved for clinical use (25). These MBs use a variety of shell materials, such as lipids, galactose, albumin and polymers (26). Some MBs have hard shells and should be strictly called 'microballoons' (27) or 'microcapsules' (28). Although the hard shells change the oscillatory and echogenic properties of MBs and affect their acoustic responses (29,30), these changes do not affect their clinical use as an ultrasound contrast agent (26). Therefore, we use the term 'microbubble' (MB) in a broad sense to refer to any microparticulate blood pool agents with a spherical core–shell structure. Similarly, the term 'nanobubble' (NB) refers to any nanoparticulate agents with a spherical core–shell structure. Both MBs and NBs can be polyethylene glycol PEGylated, surface conjugated and intravenously administered. The size difference between MBs and NBs determines their different pharmacokinetics and targeting applications. MBs may circulate in the blood stream to target the over-expressed endothelial biomarkers (31,32). NBs and nanoparticles may penetrate the endothelial barrier via the enhanced permeability and retention (EPR) effect to target the over-expressed tissue biomarkers (33).

Among various shell materials for MBs and NBs, poly(lactic acid), poly(ε-caprolactone) (PCL), poly(glycolic acid) and poly (lactide-co-glycolide) (PLGA) are of great interest because of their purity, reproducibility, biocompatibility and biodegradability. In particular, PLGA has been approved by the FDA for human therapeutic applications (34). Surface conjugated PLGA microparticles and nanoparticles have been used as carriers for targeted delivery of many imaging agents, drugs and genes (35–38). The achievable circulation lifetime of these particles is affected by the shell material, the surface coating method and the filling gas. The particle surface can be PEGylated for reduced immunogenicity and prolonged residence in the vascular system (39). With PEGylation or other surface modification methods, both microparticles and nanoparticles can circulate in body for up to several hours (25,40).

Polymer MBs and NBs can be fabricated by many methods. Double emulsion is a commonly used process (41,42). The imaging and therapeutic payloads are encapsulated in a polymer shell following four steps. First, an aqueous solution of payloads is emulsified in an organic solution of the carrier polymer to form a water-in-oil (w/o) emulsion. Second, the first emulsion is further emulsified in a large-volume of water to form a water-in-oil-in-water (w/o/w) emulsion. Third, the organic solvent is evaporated or extracted to obtain particles with a solid polymer shell. Finally, the particles are washed, centrifuged and lyophilized. The dried MBs and NBs can be refilled with heavy inert gases, such as nitrogen and perfluorocarbons (PFCs). The particle size range can be controlled by adjusting process parameters. In general, emulsification using a mechanical homogenizer followed by low-speed centrifugation will produce MBs, while emulsification using an ultrasonic homogenizer followed by high-speed centrifugation will produce NBs. PLGA MBs and NBs encapsulating various imaging and therapeutic agents have been fabricated by a modified double emulsion process (7,22,43,44). Fig. 1 shows the volume-weighted size distributions of typical MBs and NBs characterized by dynamic light scattering (22).

The double emulsion process is able to fabricate MBs and NBs with productivity and reproducibility. However, the process has low encapsulation rate, limited loading efficiency and broad size distribution. Therefore, modified emulsion systems, such as w/o/o/w (water-in-oil-in-oil-in-water) and s/o/o/w (solid-in-oil-in-oil-in-water), have been explored for the enhanced encapsulation efficiency, bioactivity and stability (45,46). Other solution-based fabrication techniques, such as emulsion diffusion, solvent displacement and salting out methods, have also been studied (42). Spray-based fabrication techniques, such as spray drying, hydrodynamic spraying and electrohydrodynamic atomization, have also been used to produce MBs and NBs with uniform size distribution and high productivity. Spray drying is a method to produce drug-loaded particles from a liquid or slurry by rapidly drying with a hot gas (47,48). The hydrodynamic spraying technique is based on hydrodynamic focusing of an inner drug and outer polymer solution emanating from a coaxial needle assembly into a two-layer compound jet (49). The electrohydrodynamic atomization process relies on the electrical shear stress to elongate the core and the shell liquid menisci formed at the outlet of coaxial capillary needles subject to an electrical field of high voltage (50–53). Optimal and reproducible control of the spray-based microencapsulation processes requires significant modeling and experimental efforts (54,55). Extrusion represents another category of fabrication processes where microencapsulated droplets are formed by feeding laminar flows of drugs, imaging agents and polymer materials through a single or a plurality of microchannel pathways directly into the continuous extraction phases (56). Commonly used extrusion systems include single pathway systems (57), multichannel systems (58) and membranes (59). Typically, the extrusion

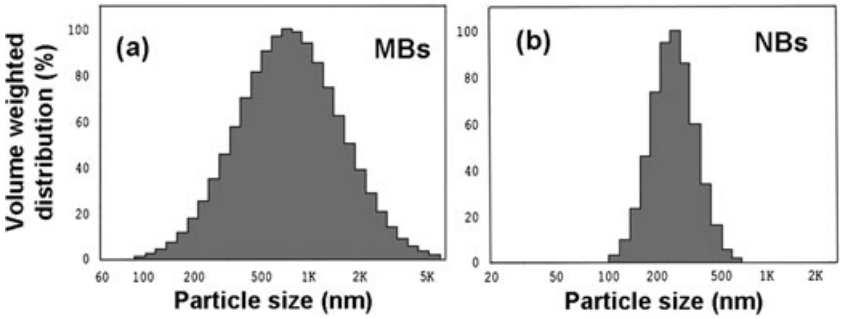

Figure 1. The size distributions of India ink encapsulated MBs (a) and NBs (b). The *x*-axis is a log scale. The average size of MBs is 1.01 ± 0.73 μm, and that of NBs is 0.29 ± 0.09 μm. Adapted from reference (22).

processes produce microparticles with uniform size distribution but with low productivity.

3. MULTIMODAL MBs AND NBs

Since photoacoustic imaging is highly sensitive to optical absorption, encapsulating highly absorbing and biocompatible optical contrast agents in MBs and NBs has technical significance. ICG is one of the first optical contrast agents approved by the FDA for clinical imaging applications (60,61). It is commonly used as a blood pool agent because of its strong binding to plasma proteins in the vascular system. The fluorescence emission peak of ICG falls in the near-infrared wavelength range, enabling deep penetration of light through thick biological tissue (17,62,63). However, quantitative analysis of ICG-enhanced optical imaging is difficult because of its short circulation half-life and inconsistent spectral characteristics owing to aggregation and protein interaction in the blood stream (64). Encapsulating ICG in PLGA MBs and NBs will prolong its circulation half-life and protect it from nonspecific molecular interactions. Previous studies have demonstrated the enhanced photo, thermal and aqueous stability by entrapping ICG in PLGA nanoparticles (65). Intravenous injection of ICG entrapped nanoparticles in healthy mice has resulted in significantly longer circulation time and increased concentration as compared with free ICG solution (38). Encapsulating ICG in PLGA MBs has yielded dual-mode contrasts for simultaneous US and fluorescence imaging (43). Since ICG is also a contrast enhancement agent in photoacoustic imaging (17), it is technically feasible to demonstrate concurrent US, photoacoustic and fluorescence imaging using ICG loaded MBs and NBs.

The gold nanoparticle (GNP) agent is another highly absorbing optical contrast agent that can be encapsulated in MBs and NBs for dual-mode photoacoustic and US imaging. GNPs have been used in many imaging and therapeutic applications because of their unique chemical and physical properties. First, GNPs are essentially inert and nontoxic (66). Second, the absorption spectrum of GNPs can be finely tuned in the near-infrared wavelength range where light can penetrate deep in biological tissue (67). Third, established techniques are available for surface mobilization, functionalization and conjugation of GNPs (68). Finally, GNPs exhibit high photostability and no photobleaching in the near-infrared wavelength range (69). GNPs with different morphologies, such as nanorods, nanospheres and nanocages, have been synthesized for contrast-enhanced photoacoustic imaging (19–21). Gold nanospheres of 20 nm have been encapsulated in a bovin serum albumin (BSA) shell of less than 200 nm following successive steps of modifying GNP surface, transferring GNPs from aqueous solution to organic solution, emulsifying GNP-loaded PFC droplets in BSA, and extruding the emulsion for more uniform particle size distribution (23). Simultaneous photoacoustic and US contrasts have been observed from the polyacrylamide phantoms with the embedment of GNP-loaded PFC droplets (23).

In addition to ICG and GNPs, other optical absorption agents, such as India ink, can also be encapsulated in MBs and NBs, as illustrated in Fig. 2. India ink-loaded MBs and NBs have been fabricated by a modified double emulsion process (22). The MBs and NBs are uniformly dispersed in gelatin phantoms and characterized by a US probe and a photoacoustic macroscope, respectively. As shown in Fig. 3, the US signals and the photoacoustic signals are positively correlated with MB and NB concentrations. In Fig. 4, a gelatin phantom with eight embedded targets of India ink MBs and NBs is clearly visible by the photoacoustic macroscope even when a piece of 18 mm thick chicken breast tissue is placed on the top of the phantom. These preliminary results suggest the technical potential of using dual-mode MBs and NBs for quantitative photoacoustic and US imaging in thick biological tissue.

Encapsulating multiple imaging agents in MBs and NBs also opens a new avenue for multimodal imaging with seamless co-registration. Multimodal imaging refers to the integration of two or more imaging modalities within a single device for simultaneous acquisition of anatomical, functional, and molecular information of biological tissue (70–72). Since individual imaging modalities only reveal a small piece of a complex puzzle in disease etiology, simultaneous acquisition of these images and seamless

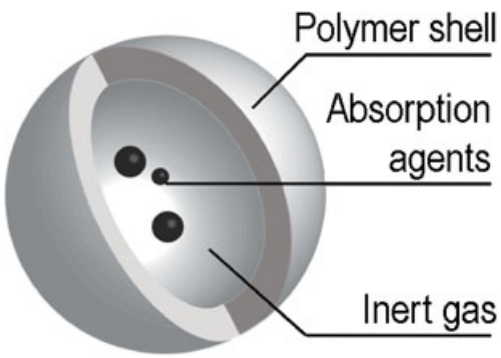

Figure 2. The schematic of polymer MBs and NBs encapsulating optical absorption contrast agents for dual-mode photoacoustic and US imaging.

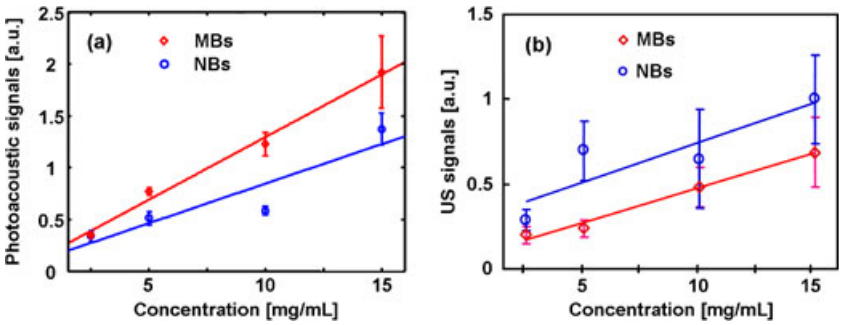

Figure 3. (a) PA signals at various MB and NB concentrations. MBs and NBs are encapsulated with India ink. (b) US signals at the same MB and NB concentrations. For both India ink encapsulated MBs and NBs, linear correlations were observed between the PA/US signals and the particle concentrations. Adapted from reference (22).

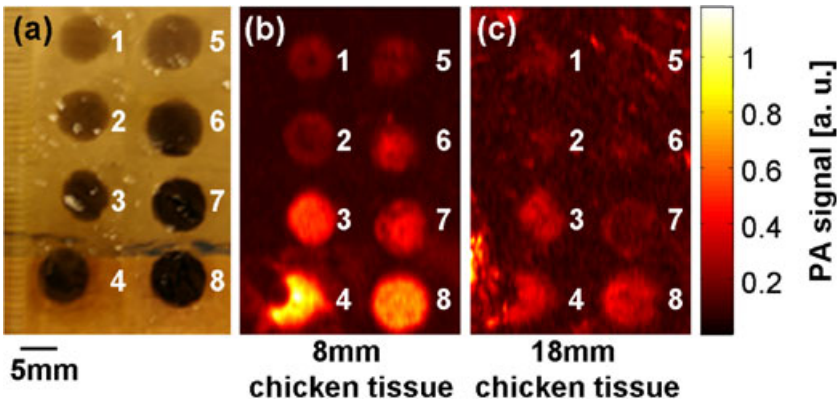

Figure 4. (a) Photograph of a phantom containing eight tumor simulators. Individual tumor simulators are homogenously dispersed with India ink encapsulated MBs and NBs at various concentrations. (b) The corresponding photoacoustic image of the phantom positioned below 8 mm of chicken breast tissues. (c) The corresponding photoacoustic image of the phantom positioned below 18 mm of chicken breast tissues. 1–4: MBs at concentrations of 2.5, 5.0, 10 and 15 mg/mL, respectively. 5–8: NBs at concentrations of 2.5, 5.0, 10 and 15 mg/mL, respectively. Adapted from reference (22).

co-registration between them have clinical significance. Clinically available multimodal imaging systems include SPECT-CT (integration of single photon emission computed tomography and computed tomography) (73) and PET-CT (integration of positron emission tomography and CT) (74). Other emerging multimodal imaging techniques include MRI-PET (integration of magnetic resonance imaging and PET) (75), MRI-NIR (integration of MRI and near infrared imaging) (61), NIR-US (integration of NIR and US imaging) (76), mammography-NIR (integration of mammography and NIR imaging) (77), PAT-US (integration of photoacoustic tomography and US imaging) (78) and PAM-OCT (integration of photoacoustic microscopy and optical coherence tomography) (79). As a portable and noninvasive imaging tool with molecular sensitivity, favorable spatial resolution, and large measurement depth, photoacoustic imaging has the potential to play an important role in multimodal imaging. Synthesizing multimodal MBs and NBs is the first step toward quantitative multimodal imaging that seamlessly integrates photoacoustic imaging with other modalities for preoperative diagnosis, intraoperative therapeutic guidance and postoperative outcome assessment.

4. MULTIFUNCTIONAL DISEASE-TARGETING MBs AND NBs

Since photoacoustic imaging is highly sensitive to tissue chromophores, it has been primarily used for noninvasive detection of microvessels and tissue functional parameters (16,80,81). The emergence of the multifunctional MB and NB agents extends the application of photoacoustic imaging from nonspecific functional imaging to disease-specific molecular imaging. Multifunctional MBs and NBs are agents that integrate multiple disease-targeting, imaging and therapeutic functions. PEGylated and surface modified MBs and NBs are able to target various disease biomarkers with high binding affinity (7,39). Previous studies have demonstrated that individual MBs can be detected by a clinical US probe (82). Similar technical potential exists for photoacoustic imaging of individual MBs or NB clusters if the bubbles are loaded with strong chromophores at high concentration. Loading imaging and therapeutic agents in MBs and NBs may also facilitate image-guided drug delivery and combinatory therapies (83,84).

PLGA MBs and NBs can be conjugated with a wide variety of disease-targeting ligands, such as antibodies, peptides, polysaccharides, aptamers and drugs alone or in combination, for disease-specific imaging and therapeutic applications (85). The MBs can be conjugated to target the circulating and endothelium over-expressed biomarkers, such as selectins, $\alpha_v\beta_3$ or $\alpha_5\beta_1$ integrins, glycoprotein (GP) IIb/IIIa, intracellular adhesion molecule 1 (ICAM-1), and vascular endothelial growth factor receptor 2 (VEGFR2) (86). One example is to conjugate MBs with anti-VEGFR2 antibodies for *in vivo* ultrasonic detection of tumor angiogenesis and continuous monitoring of tumor vascular response to therapy (32,87,88). The NBs can be conjugated to target the over-expressed tissue biomarkers. One example is to conjugate NBs with anti-TAG-72 antibodies, such as CC49, to target TAG-72,

a human mucin-like glycoprotein complex over-expressed in many epithelial-derived cancers, including colorectal, pancreatic, gastric, prostate, breast, ovarian and lung cancers (89). We have previously encapsulated Texas Red in PLGA NBs and conjugated them with CC49 antibody to target the LS174T human colorectal cancer cells (7). As shown in Fig. 5, NBs conjugated with CC49 can effectively target the cancer cells through both a one-step and a three-step binding processes. In comparison, bare TexasRed NBs without surface conjugation do not bind with cancer cells. The above targeting strategies can be used to fabricate multi-functional MBs and NBs for disease-specific photoacoustic imaging.

5. ACTIVATABLE MBs AND NBs

Activatable MBs and NBs are those that can be activated by external energy sources. Typically, activatable MBs and NBs encapsulate PFC droplets in a polymer shell. PFCs represent a group of fluorocarbon compounds with biocompatibility, chemical stability, low solubility and large density compared with many other gases. They have been used clinically as an oxygen carrier in blood substitutes and a filler gas in US contrast agents (90–92). The PFC compounds have a wide range of boiling points and can be mixed at different ratios for controllable phase shift mediated by an external energy (93). Upon the exposure of tone-burst ultrasound, superheated PFC droplets can be vaporized into gas bubbles, enabling many therapeutic and diagnostic applications (94). Optical contrast agents can be encapsulated in these activatable MBs and NBs so that the energy-induced evaporation and volumetric expansion can be detected by multiple imaging tools, such as US, photoacoustic and fluorescence imaging. Therapeutic agents can also be encapsulated for image-guided drug delivery (95).

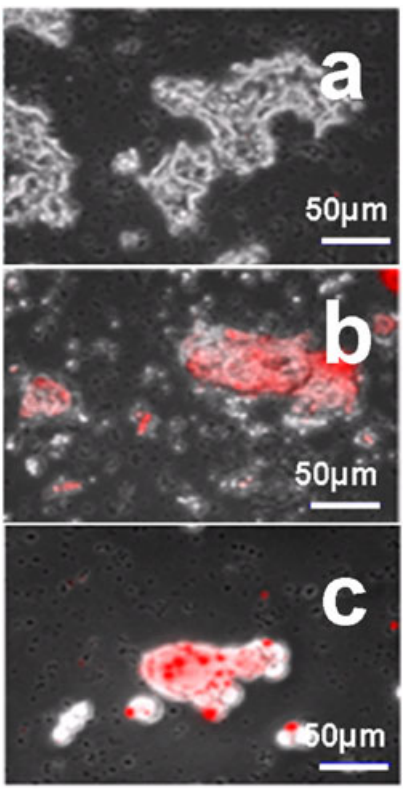

Figure 5. Fluorescence microscopic images of LS174T cancer cell cultures after different targeting processes for PLGA NBs. Texas Red dye is encapsulated in NBs. (a) Cells after applying bare Texas Red NBs without surface conjugation (control). (b) Cells after successive application of biotinylated HuCC49ΔCH2 antibody, streptavidin, and biotinylated NBs (three-step targeting). (c) Cells after applying NBs conjugated with HuCC49ΔCH2 antibody (one-step targeting). NBs bind with cancer cells well after both three-step and one-step targeting processes. In comparison, bear NBs do not bind with cancer cells. Adapted from reference (7) with modification.

A commonly used method to fabricate activatable MBs and NBs is modified emulsion and evaporation (95–97). The process consists of successive steps of dissolving the shell material in a volatile organic solvent, mixing the solution with a PFC compound and a surfactant, emulsification, organic solvent evaporation and centrifugation. The precipitate collected from the process is then washed multiple times to obtain activatable MBs and NBs. The bubble morphology, size and shell thickness parameters can be controlled by adjusting the type and the mixing ratio of different shell, solvent, surfactant and PFC materials, the power and duration of emulsification, and the centrifugation/filtering conditions. If the evaporation rate of the organic solvent is close to that of the PFC compound, other encapsulation processes, such as hydrodynamic spray and microchannel extrusion, can be used (52,56).

Two possible applications for activatable MBs and NBs are image-guided drug delivery (for activatable NBs) and ablation margin assessment (for activatable MBs). Image-guided drug delivery with drug-loaded polymer micelles and activatable NBs has been explored for combinatory tumor imaging and targeted chemotherapy (8). Micelles of a biodegradable copolymer (e.g., PEG-PLLA or PEG-PCL) were fabricated by a solvent exchange technique. PFC compounds (e.g. perfluoropentane) were encapsulated in the NBs of the same copolymer shell by a nanoemulsion process. Lipophilic drugs can be loaded in both the micelle cores and the walls of the activatable NBs by emulsification. Hydrophilic drugs can be loaded by other microencapsulation processes such as hydrodynamic spray and microchannel extrusion. The combinatory tumor imaging and targeted chemotherapy technique is based on the following hypotheses: (1) after intravenous injection, drug-loaded micelles and NBs will penetrate the defective tumor microvasculature and accumulate in the tumor tissue; (2) the PFC compound loaded in NBs will be evaporated by external energy sources through either body heat or US pulses, causing volumetric expansion, coalescence, or cavitation of NBs; and (3) the conversion of NBs into MBs mediated by external energy sources will introduce significant contrast ehancement for image-guided drug release. The above hypotheses have been partially verified by *in vitro* and *in vivo* tests. In one experiment, a closed plastic capillary filled with the activatable NBs was subject to a repetitive heating/cooling/heating cycle. The process was monitored by a microscope and plotted in Fig. 6. As shown in the figure, the cyclic temperature fluctuation introduces both reversible and irreversible changes in bubble morphology. Significant coalescence can be observed after overheating the sample to hyperthermia temperatures. US-mediated release of doxorubicin from MBs and internalization by the cells has also been demonstrated *in vitro* (95).

In addition to image-guided drug delivery, the heat-induced coalescence and expansion of activatable MBs can also be used for intraoperative assessment of ablation margin during thermal ablation therapies (98). Previous studies have demonstrated that PFC droplets can be superheated and remain stable above their

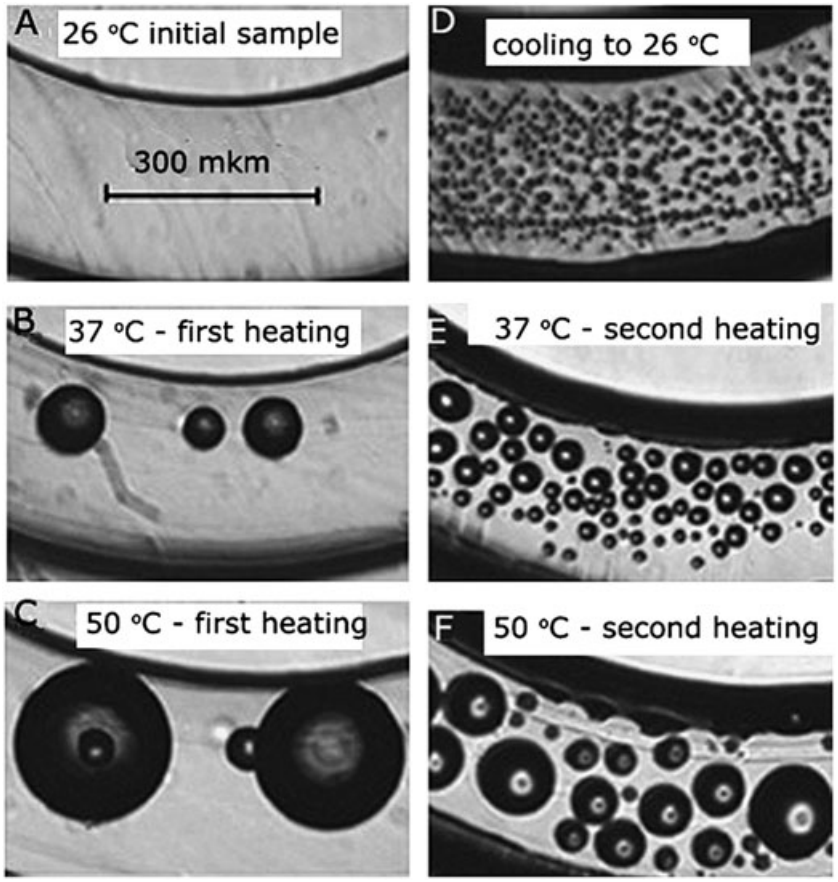

Figure 6. Microscopic images of doxorubicin and perfluoropentane loaded PEG-PLLA NBs in a closed plastic capillary of a snake mixer slide. (A) At 26 °C, NBs were not resolved at the highest available magnification. (B, C) Upon heating to 37 and 50 °C, respectively, large bubbles grew by attracting and coalescing with small ones. (D) After the sample was cooled back to room temperature, the initial structure was not restored and a large number of small MBs were formed via disintegration of large microbubbles and PFP condensation inside the bubble walls. (E, F) Microscopic images taken during a second heating step at 37 and 50 °C, respectively; the growth of large MBs through attraction and coalescence with small ones was manifested by a progressive decrease in the number of small MBs. Adapted from reference (8).

natural boiling points (94,99,100). We have also observed the activation of PFC-loaded MBs at a much lower temperature close to the PFC boiling point (97). The different evaporation thresholds for PFC droplets and PFC-loaded MBs may be associated with the different thickness and mechanical properties of the shell materials, as well as the possible nucleus formation inside the surface of the PLGA shell. The heat activation of PFC-loaded MBs may have clinical significance because no intraoperative imaging tool is available yet for direct assessment of tissue coagulation necrosis during a cancer ablation procedure. Thermal ablation destroys tumor tissue by localized deposition of thermal energy that causes protein denaturation and coagulation necrosis (101). Clinical advantages of thermal ablation include minimal trauma, minimal complication, outpatient treatment, fast recovery and fast return to normal activities. However, the widespread use of these minimally invasive therapeutic option is hindered by controversial issues and concerns regarding clinical safety, long-term local recurrence rate and disease-free survival. A primary reason for these concerns is the lack of effective imaging tools for intraoperative margin assessment. In this regard, US imaging alone cannot detect the zone of ablation effectively because of the hyperechoic artifacts associated with gas bubble formation and 'steam popping' (102–104). Other imaging methods, such as MRI, estimate ablation-induced thermal damage indirectly based on continuous monitoring of tissue temperature histories (105,106). The reliability of these indirect methods is limited by the modeling error, the accumulative measurement error and the cooling down effect of the ablated tissue. Activatable MBs may provide multimodal imaging contrasts for reliable assessment of ablation margin. The activatable MBs for this application are called heat-sensitive MBs because they are sensitive to ablation-induced thermal energy deposition. The application of heat-sensitive MBs is based on the following hypotheses: (1) MBs with a specific design of size, shell thickness and PFC encapsulation rate will be activated at the lethal thermal dose corresponding to the irreversible tissue thermal damage; (2) the evaporation of PFC droplets loaded in activatable MBs will cause volumetric expansion, latent heat, mass transfer and scattering changes that can be detected by US and optical imaging tools; (3) encapsulating highly absorbing contrast agents in heat-sensitive MBs will facilitate ablation margin confirmation using multiple imaging modalities so that the effect of nonspecific gas bubbles and other hyperechoic artifacts can be minimized; and (4) after thermal activation, the heat-sensitive MBs will remain strong multimodal imaging contrasts for a long time, enabling ablation margin assessment regardless of tissue temperature fluctuation and other spatial and temporal artifacts. Heat-sensitive MBs have been fabricated by a modified emulsion-evaporation process and tested in both agar agar gel phantoms and *ex vivo* tissue models (97). Fig. 7 shows the temperature distribution acquired by a

thermal camera and the corresponding hyperechoic region acquired by a clinical US probe in a piece of porcine tissue that is ablated by a miniature cartridge heater. Microscopic imaging of the phantom further confirmed the coincidence between the ultrasonically hyperechoic region and the ablation-induced morphologic changes in the phantom, indicating the technical feasibility of using heat-sensitive MBs for ablation margin assessment. MB enhanced ablation margin assessment has also been demonstrated in various *ex vivo* tissue models, such as perfused porcine kidneys, porcine tissue and porcine pancreas. In one experiment, the aqueous suspension of heat-sensitive MBs was injected into eight locations around a circular line in a piece of porcine tissue, as shown in Fig. 8(a). All eight hyperechoic spots were clearly visible by a clinical US probe after heating the tissue to the coagulation necrosis temperature (Fig. 8d). The eight hyperechoic spots lasted for over an hour after the tissue was cooled down (Fig. 8e), indicating the technical feasibility of detecting ablation-induced tissue coagulation necrosis regardless of the transient tissue temperature changes and artifacts.

Although activatable MBs and NBs have not been optimized for photoacoustic imaging yet, the rationale of using them for contrast enhanced photoacoustic imaging of ablation margin has been supported by several previous studies. In the field of atmospheric science, the change of photoacoustic signals by latent heat and mass transfer in response to water droplet evaporation has been theoretically studied and experimentally detected (107,108). In the field of biomedical imaging, the photoacoustic technique has been used to detect tissue temperature changes with a measurement sensitivity of 0.15 °C and a temporal resolution of 2 s (109,110). To enhance the photoacoustic sensitivity of activatable MBs and NBs at the presence of irreversible tissue thermal damage, it is important to optimize the bubble thickness and morphology, to increase the dye encapsulation efficiency, and to control the thermal energy threshold for bubble activation.

6. OPPORTUNITIES AND CHALLENGES

MBs and NBs represent an enabling technology for many innovative applications in the field of photoacoustic imaging. First of all, highly absorbing optical contrast agents can be loaded in MBs and NBs for strong photoacoustic contrast, reduced nonspecific molecular interaction, improved stability and prolonged circulation lifetime. Second, multiple imaging agents can be encapsulated in MBs and NBs for multimodal imaging of tissue structural and functional anomalies. By using MBs and NBs with multimodal imaging contrasts, photoacoustic imaging can be accurately co-registered with other imaging modalities, such as US, OCT, diffuse optical tomography, fluorescence imaging, MRI, CT and PET. Third, the surface of MBs and NBs can be PEGylated and conjugated for disease-specific photoacoustic imaging. Surface modified MBs can circulate in blood stream to target various disease markers in the vascular space (86). Surface modified NBs can circulate in blood stream, penetrate the leaky tumor vasculature via the

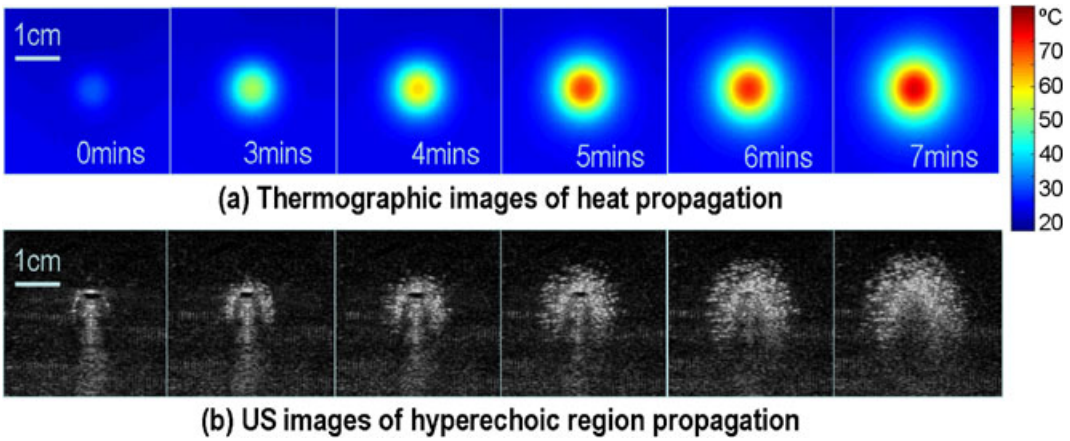

Figure 7. Thermographic and US images simultaneously acquired from a solid gel phantom as the phantom is ablated by a miniature cartridge heater. The phantom is homogenously dispersed with heat-sensitive microbubbles. (a) Thermographic images show the propagation of heat; (b) US images show the propagation of an ultrasonically hyperechoic region corresponding to the activation of heat-sensitive microbubbles.

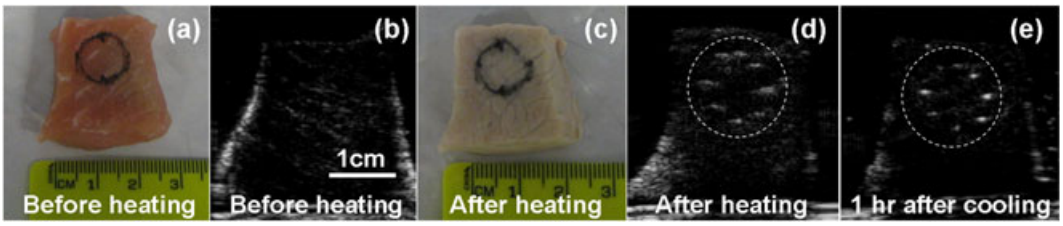

Figure 8. Photographic and ultrasound images of a piece of porcine tissue before and after being heated to tissue coagulation temperature. (a) Photographic image before heating. Heat-sensitive MBs are injected at eight locations along the black circular mark. (b) Ultrasound image before heating shows no significant hyperechoic spots. (c) Photographic image of the tissue after being placed in a 55 °C water bath for 10 min. (d) Ultrasound image after heating shows eight hyperechoic spots (within the dotted circle) corresponding to eight locations where heat-sensitive MBs were injected. (e) Ultrasound image acquired after cooling the sample for 1 h. The eight hyperechoic spots are still clearly visible. Adapted from reference (97).

EPR effect and target various disease markers in the tissue space (33). Fourth, multiple imaging agents and combinatory drugs can be encapsulated in MBs and NBs for image-guided synergistic therapy. Finally, systemic or regional delivery of heat-sensitive MBs will enable intraoperative assessment of zone of ablation during a thermal ablation procedure. Therapeutic agents can also be loaded in heat-sensitive MBs for thermally activated release of adjuvant therapy. To facilitate successful translation from the benchtop to the bedside, the design of MB and NB contrast agents for photoacoustic imaging should consider the following requirements: (1) materials used to construct MBs and NBs should have no adverse effects on the biological system; (2) MBs and NBs should have consistent and reproducible size, thickness and encapsulation rate to facilitate quantitative imaging; (3) MBs and NBs should have strong and consistent optical contrasts minimally affected by degradation, photobleaching and physiologic fluctuations; and (4) MBs and NBs should have relatively long shelf-life and can be calibrated against a traceable standard.

As a new field with great promise, the MB- and NB-enhanced photoacoustic imaging technique also faces many challenges. First of all, commonly used microfabrication processes such as double emulsion have a relatively low encapsulation rate. Therefore, dye-loaded MBs and NBs do not have sufficient absorption contrasts to facilitate photoacoustic imaging in thick biological tissue. Spray-based micro and nanoencapsulation processes may produce MBs and NBs with greater encapsulation rates. However, many of these processes are still under development and require significant research efforts on mathematical modeling and process control. Second, commonly used microfabrication processes such as double emulsion produce MBs and NBs with a large range of size distributions. The nonuniformity of MBs and NBs will not only affect their optical and acoustic properties but also limit the achievable accuracy for contrast enhanced photoacoustic imaging. Although additional cycles of centrifugation and filtering may yield more uniform MBs and NBs, the process has a significantly low productivity. Third, quantitative photoacoustic imaging is still not feasible owing to the lack of standardization. Traceable calibration standards and testing protocols have to be established in order to quantify critical performance parameters, such as limit of detection, optical stability, signal-to-noise ratio, linearity range, dynamic range and reproducibility. Better understanding about the mechanism for MB and NB enhanced photoacoustic imaging is necessary in order to facilitate engineering design and optimization. Fourth, future *in vivo* applications of MB and NB agents may be hindered by insufficient disease-specific accumulation. Although MB and NB circulation in the vascular system can be significantly prolonged by PEGylation, the achievable disease-specific deposition of these particles is limited by many physical and physiologic barriers (111). To ensure *in vivo* photoacoustic imaging with high accuracy and sensitivity, it is important to transport and deliver disease-targeting MBs and NBs with high efficiency. One possible strategy is to enhance the disease-binding affinity by multivalent conjugates (112). Another possible strategy is to use external energy sources such as US pulses to facilitate active transport of drugs and contrast agents across the endothelial barrier (113). Finally, regulatory approval may present another hurdle for clinical imaging and image-guided therapeutic applications. Although individual composition materials for MBs and NBs are biocompatible and biodegradable, extensive preclinical studies are still required to characterize the biodistribution, pharmacokinetic and toxicity profiles of the MB and NB agents and to prepare for FDA IND (investigational new drug) application as well as pilot clinical trials.

7. SUMMARY AND OUTLOOK

Originally used as US contrast enhancement agents and drug delivery carriers, polymer MBs and NBs can potentially play an important role in photoacoustic imaging. This paper describes the fabrication and application aspects of polymer MBs and NBs. MBs and NBs can be fabricated by many processes, such as double emulsion, emulsion evaporation, solvent displacement, spray drying, hydrodynamic spraying, electrohydrodynamic atomization and microchannel extrusion. Highly absorbing optical contrast agents, such as GNPs, India ink and ICG, can be encapsulated in MBs and NBs for simultaneous photoacoustic and US imaging. Many other contrast agents can also be encapsulated for multimodal imaging with accurate co-registration. The surface of MBs and NBs can be PEGylated and conjugated for disease-specific targeting with reduced immunogenicity and prolonged circulation lifetime. Activatable MBs and NBs can be fabricated by encapsulating low boiling point PFC compounds in a polymer shell. Applying external energy to these MBs and NBs may trigger the PFC phase shift, introducing volumetric expansion or cavitation for multiple imaging and therapeutic applications. Example clinical applications may include ablation margin assessment (for activatable MBs) and image-guided drug delivery (for activatable NBs).

MB and NB enhanced photoacoustic imaging is a new research field with great potential. Further improvement in process control and engineering optimization is required for the production of monodisperse MBs and NBs with high encapsulation rate, productivity and reproducibility. Traceable calibration standards and testing protocols need to be established for MB and NB enhanced quantitative photoacoustic imaging. Extensive technology development, preclinical validation and regulatory approval are necessary before the MB and NB agent can be used for contrast enhanced photoacoustic imaging in a clinical setting.

REFERENCES

1. Sanders RC, Winter TC (eds). Clinical Sonography: a Practical Guide. Lippincott Williams & Wilkins: Philadelphia, PA, 2007.
2. Quaia E. Microbubble ultrasound contrast agents: an update. Eur Radiol 2007; 17(8): 1995–2008.
3. Nanda NC, Carstensen C (eds). Echo-enhancing Agents: Safety. Kluwer Academic Publishers: Boston, 1995.
4. Kiessling F. Science to practice: the dawn of molecular US imaging for clinical cancer imaging. Radiology 2010; 256(2): 331–333.
5. Ferrara K, Pollard R, Borden M. Ultrasound microbubble contrast agents: fundamentals and application to gene and drug delivery. Annu Rev Biomed Eng 2007; 9: 415–447.
6. Klibanov AL. Microbubble contrast agents: targeted ultrasound imaging and ultrasound-assisted drug-delivery applications. Invest Radiol 2006; 41(3): 354–362.
7. Xu JS, Huang J, Qin R, Hinkle GH, Povoski SP, Martin EW, Xu RX. Synthesizing and binding dual-mode poly (lactic-co-glycolic acid) (PLGA) nanobubbles for cancer targeting and imaging. Biomaterials 2010; 31(7): 1716–1722.
8. Rapoport N, Gao Z, Kennedy A. Multifunctional nanoparticles for combining ultrasonic tumor imaging and targeted chemotherapy. J Natl Cancer Inst 2007; 99(14): 1095–1106.
9. Marsh JN, Partlow KC, Abendschein DR, Scott MJ, Lanza GM, Wickline SA. Molecular imaging with targeted perfluorocarbon nanoparticles: quantification of the concentration dependence of contrast enhancement for binding to sparse cellular epitopes. Ultrasound Med Biol 2007; 33(6): 950–958.

10. Wang LV. Prospects of photoacoustic tomography. Med Phys 2008; 35(12): 5758–5767.
11. Rosencwaig A, Gersho A. Theory of the photoacoustic effect in solids. J Appl Phys 1976; 47: 64–69.
12. Zhang HF, Maslov K, Wang LV. In vivo imaging of subcutaneous structures using functional photoacoustic microscopy. Nat Protoc 2007; 2(4): 797–804.
13. Maslov K, Zhang HF, Hu S, Wang LV. Optical-resolution photoacoustic microscopy for in vivo imaging of single capillaries. Opt Lett 2008; 33(9): 929–931.
14. Xie Z, Jiao S, Zhang HF, Puliafito CA. Laser-scanning optical-resolution photoacoustic microscopy. Opt Lett 2009; 34(12): 1771–1773.
15. Xu M, Wang LV. Universal back-projection algorithm for photoacoustic computed tomography. Phys Rev E Stat Nonlin Soft Matter Phys 2005; 71(1 Pt 2): 016706.
16. Wang X, Xie X, Ku G, Wang LV, Stoica G. Noninvasive imaging of hemoglobin concentration and oxygenation in the rat brain using high-resolution photoacoustic tomography. J Biomed Opt 2006; 11(2): 024015.
17. Ku G, Wang LV. Deeply penetrating photoacoustic tomography in biological tissues enhanced with an optical contrast agent. Opt Lett 2005; 30(5): 507–509.
18. Song KH, Stein EW, Margenthaler JA, Wang LV. Noninvasive photoacoustic identification of sentinel lymph nodes containing methylene blue in vivo in a rat model. J Biomed Opt 2008; 13(5): 054033.
19. Song KH, Kim C, Cobley CM, Xia Y, Wang LV. Near-infrared gold nanocages as a new class of tracers for photoacoustic sentinel lymph node mapping on a rat model. Nano Lett 2009; 9(1): 183–188.
20. Wang B, Yantsen E, Larson T, Karpiouk AB, Sethuraman S, Su JL, Sokolov K, Emelianov SY. Plasmonic intravascular photoacoustic imaging for detection of macrophages in atherosclerotic plaques. Nano Lett 2009; 9(6): 2212–2217.
21. Li PC, Wang CR, Shieh DB, Wei CW, Liao CK, Poe C, Jhan S, Ding AA, Wu YN. In vivo photoacoustic molecular imaging with simultaneous multiple selective targeting using antibody-conjugated gold nanorods. Opt Express 2008; 16(23): 18605–18615.
22. Kim C, Qin R, Xu JS, Wang L, Xu RX. Ultrasound and photoacoustic dual-modal imaging of thick biological tissue with microbubble enhancement. J Biomed Opt 2010; 15(1): 010510.
23. Wilson K, Homan K, Emelianov S. Photoacoustic and ultrasound imaging contrast enhancement using a dual contrast agent. Proceedings of SPIE 7564(75642P), 2009.
24. Microbubbles. http://en.wikipedia.org/wiki/Microbubbles (accessed 25 January 2011).
25. Correas JM, Bridal L, Lesavre A, Mejean A, Claudon M, Helenon O. Ultrasound contrast agents: properties, principles of action, tolerance, and artifacts. Eur Radiol 2001; 11(8): 1316–1328.
26. Lindner JR. Microbubbles in medical imaging: current applications and future directions. Nat Rev Drug Discov 2004; 3(6): 527–532.
27. Schneider M, Bussat P, Barrau MB, Arditi M, Yan F, Hybl E. Polymeric microballoons as ultrasound contrast agents. Physical and ultrasonic properties compared with sonicated albumin. Invest Radiol 1992; 27(2): 134–139.
28. El-Sherif DM, Wheatley MA. Development of a novel method for synthesis of a polymeric ultrasound contrast agent. J Biomed Mater Res A 2003; 66(2): 347–355.
29. Straub JA, Chickering DE, Church CC, Shah B, Hanlon T, Bernstein H. Porous PLGA microparticles: AI-700, an intravenously administered ultrasound contrast agent for use in echocardiography. J Control Release 2005; 108(1): 21–32.
30. Wheatley MA, Forsberg F, Oum K, Ro R, El-Sherif D. Comparison of in vitro and in vivo acoustic response of a novel 50:50 PLGA contrast agent. Ultrasonics 2006; 44(4): 360–367.
31. Ellegala DB, Leong-Poi H, Carpenter JE, Klibanov AL, Kaul S, Shaffrey ME, Sklenar J, Lindner JE. Imaging tumor angiogenesis with contrast ultrasound and microbubbles targeted to alpha(v)beta3. Circulation 2003; 108(3): 336–341.
32. Pochon S, Tardy I, Bussat P, Bettinger T, Brochot J, von Wronski M, Passantino L, Schneider M. BR55: a lipopeptide-based VEGFR2-targeted ultrasound contrast agent for molecular imaging of angiogenesis. Invest Radiol 2010; 45(2): 89–95.
33. Brannon-Peppas L, Blanchette JO. Nanoparticle and targeted systems for cancer therapy. Adv Drug Deliv Rev 2004; 56(11): 1649–1659.
34. Shive MS, Anderson JM. Biodegradation and biocompatibility of PLA and PLGA microspheres. Adv Drug Deliv Rev 1997; 28(1): 5–24.
35. Betancourt T, Brown B, Brannon-Peppas L. Doxorubicin-loaded PLGA nanoparticles by nanoprecipitation: preparation, characterization and in vitro evaluation. NanomedICINE 2007; 2(2): 219–232.
36. Bejjani RA, BenEzra D, Cohen H, Rieger J, Andrieu C, Jeanny JC, Gollomb G, Behar-Cohen FF. Nanoparticles for gene delivery to retinal pigment epithelial cells. Mol Vis 2005; 11: 124–132.
37. Bala I, Hariharan S, Kumar MN. PLGA nanoparticles in drug delivery: the state of the art. Crit Rev Ther Drug Carrier Syst 2004; 21(5): 387–422.
38. Saxena V, Sadoqi M, Shao J. Polymeric nanoparticulate delivery system for Indocyanine green: biodistribution in healthy mice. Int J Pharm 2006; 308(1–2): 200–204.
39. Betancourt T, Byrne JD, Sunaryo N, Crowder SW, Kadapakkam M, Patel S, Casciato S, Brannon-Peppas L. PEGylation strategies for active targeting of PLA/PLGA nanoparticles. J Biomed Mater Res A 2009; 91(1): 263–276.
40. Esmaeili F, Ghahremani MH, Esmaeili B, Khoshayand MR, Atyabi F, Dinarvand R. PLGA nanoparticles of different surface properties: preparation and evaluation of their body distribution. Int J Pharm 2008; 349(1–2): 249–255.
41. Jain RA. The manufacturing techniques of various drug loaded biodegradable poly(lactide-co-glycolide) (PLGA) devices. Biomaterials 2000; 21(23): 2475–2490.
42. Astete CE, Cabliov CM. Synthesis and characterization of PLGA nanoparticles. J Biomater Sci Polym Ed 2006; 17(3): 247–289.
43. Xu R, Huang J, Xu J, Sun D, Hinkle G, Edward J, Martin W, Povoski S. Fabrication of indocyanine green encapsulated biodegradable microbubbles for structural and functional imaging of cancer. J Biomed Opt 2009; 14(3): 034020.
44. Zhang L, Xu JS, Sanders VM, Letson AD, Roberts CJ, Xu RX. Multifunctional microbubbles for image-guided antivascular endothelial growth factor therapy. J Biomed Opt 2010; 15(3): 030515.
45. Zheng W. A water-in-oil-in-oil-in-water (W/O/O/W) method for producing drug-releasing, double-walled microspheres. Int J Pharm 2009; 374(1–2): 90–95.
46. Yuan W, Wu F, Guo M, Jin T. Development of protein delivery microsphere system by a novel S/O/O/W multi-emulsion. Eur J Pharm Sci 2009; 36(2–3): 212–218.
47. Cal K, Sollohub K. Spray drying technique. I: Hardware and process parameters. J Pharm Sci 2010; 99(2): 575–586.
48. Sollohub K, Cal K. Spray drying technique: II. Current applications in pharmaceutical technology. J Pharm Sci 2010; 99(2): 587–597.
49. Snider C, Lee SY, Yeo Y, Gregori GJ, Robinson JP, Park K. Microenvironment-controlled encapsulation (MiCE) process: effects of PLGA concentration, flow rate, and collection method on microcapsule size and morphology. Pharm Res 2008; 25(1): 5–15.
50. Farook U, Stride E, Edirisinghe MJ, Moaleji R. Microbubbling by co-axial electrohydrodynamic atomization. Med Biol Eng Comput 2007; 45(8): 781–789.
51. Jaworek A, Sobczyk AT. Electrospraying route to nanotechnology: an overview. J Electrostat 2008; 66(3–4): 197–219.
52. Loscertales IG, Barrero A, Guerrero I, Cortijo R, Marquez M, Ganan-Calvo AM. Micro/nano encapsulation via electrified coaxial liquid jets. Science 2002; 295(5560): 1695–1698.
53. Enayati M, Ahmad Z, Stride E, Edirisinghe M. One-step electrohydrodynamic production of drug-loaded micro- and nanoparticles. J R Soc Interface 2010; 7(45): 667–675.
54. Chen X, Jia L, Yin X, Cheng J. Spraying modes in coaxial jet electrospray with outer driving liquid. Physics of fluids 2005; 17: 032101.
55. Higuera FJ. Stationary coaxial electrified jet of a dielectric liquid surrounded by a conductive liquid. Phys Fluids 2007; 19: 012102.
56. Freitas S, Merkle HP, Gander B. Microencapsulation by solvent extraction/evaporation: reviewing the state of the art of microsphere preparation process technology. J Control Release 2005; 102(2): 313–332.
57. Amsden B. The production of uniformly sized polymer microspheres. Pharm Res 1999; 16(7): 1140–1143.
58. Freitas S, Walz A, Merkle HP, Gander B. Solvent extraction employing a static micromixer: a simple, robust and versatile technology for the microencapsulation of proteins. J Microencapsul 2003; 20(1): 67–85.

59. Shiga K, Muramatsu N, Kondo T. Preparation of poly(D,L-lactide) and copoly(lactide-glycolide) microspheres of uniform size. J Pharm Pharmacol 1996; 48(9): 891–895.
60. Benson RC, Kues HA. Fluorescence properties of indocyanine green as related to angiography. Phys Med Biol 1978; 23(1): 159–163.
61. Ntziachristos V, Yodh AG, Schnall M, Chance B. Concurrent MRI and diffuse optical tomography of breast after indocyanine green enhancement. Proc Natl Acad Sci USA 2000; 97(6): 2767–2772.
62. Corlu A, Choe R, Durduran T, Rosen MA, Schweiger M, Arridge SR, Schnall MD, Yodh AG. Three-dimensional in vivo fluorescence diffuse optical tomography of breast cancer in humans. Opt Express 2007; 15(11): 6696–6716.
63. Kupriyanov VV, Nighswander-Rempel S, Xiang B. Mapping regional oxygenation and flow in pig hearts in vivo using near-infrared spectroscopic imaging. J Mol Cell Cardiol 2004; 37(5): 947–957.
64. Desmettre T, Devoisselle JM, Mordon S. Fluorescence properties and metabolic features of indocyanine green (ICG) as related to angiography. Surv Ophthalmol 2000; 45(1): 15–27.
65. Saxena V, Sadoqi M, Shao J. Enhanced photo-stability, thermal-stability and aqueous-stability of indocyanine green in polymeric nanoparticulate systems. J Photochem Photobiol B 2004; 74(1): 29–38.
66. Connor EE, Mwamuka J, Gole A, Murphy CJ, Wyatt MD. Gold nanoparticles are taken up by human cells but do not cause acute cytotoxicity. Small 2005; 1(3): 325–327.
67. Link S, El-Sayed MA. Size and temperature dependence of the plasmon absorption of colloidal gold nanoparticles. J Phys Chem B 1999; 103(42): 4212–4217.
68. Liao H, Hafner JH. Gold nanorod bioconjugates. Chem Mater 2005; 17: 4636–4641.
69. Skirtach AG, Munoz Javier A, Kreft O, Kohler K, Piera Alberola A, Mohwald H, Parak WJ, Sukhorukov GB. Laser-induced release of encapsulated materials inside living cells. Angew Chem Int Ed Engl 2006; 45(28): 4612–4617.
70. Townsend DW. Multimodality imaging of structure and function. Phys Med Biol 2008; 53(4): R1–R39.
71. Hendee WR, Gazelle GS. Biomedical Imaging Research Opportunities Workshop III: a white paper. Ann Biomed Eng 2006; 34(2): 188–198.
72. Hendee WR, Banovac F, Carson PL, DeFronzo RA, Eckelman WC, Fullerton GD, Larson SM, McLennan G, Welch MJ. Biomedical Imaging Research Opportunities Workshop IV: a white paper. Med Phys 2007; 34(2): 673–679.
73. Lang TF, Hasegawa BH, Liew SC, Brown JK, Blankespoor SC, Reilly SM, Gingold EL, Cann CE. Description of a prototype emission-transmission computed tomography imaging system. J Nucl Med 1992; 33(10): 1881–1887.
74. Beyer T, Townsend DW, Brun T, Kinahan PE, Charron M, Roddy R, Jerin J, Young J, Byars L, Nutt R. A combined PET/CT scanner for clinical oncology. J Nucl Med 2000; 41(8): 1369–1379.
75. Hammer BE, Christensen NL, Heil BG. Use of a magnetic field to increase the spatial resolution of positron emission tomography. Med Phys 1994; 21(12): 1917–1920.
76. Zhu Q, Conant E, Chance B. Optical imaging as an adjunct to sonograph in differentiating benign from malignant breast lesions. J Biomed Opt 2000; 5(2): 229–236.
77. Li A, Miller EL, Kilmer ME, Brukilacchio TJ, Chaves T, Stott J, Zhang Q, Wu T, Chorlton M, Moore RH, Kopans DB, Boas DA. Tomographic optical breast imaging guided by three-dimensional mammography. Appl Opt 2003; 42(25): 5181–5190.
78. Karpiouk AB, Aglyamov SR, Mallidi S, Shah J, Scott WG, Rubin JM, Emelianov SY. Combined ultrasound and photoacoustic imaging to detect and stage deep vein thrombosis: phantom and ex vivo studies. J Biomed Opt 2008; 13(5): 054061.
79. Jiao S, Xie Z, Zhang HF, Puliafito CA. Simultaneous multimodal imaging with integrated photoacoustic microscopy and optical coherence tomography. Opt Lett 2009; 34(19): 2961–2963.
80. Hoelen CGA, de Mul EFM, Pongers R, Dekker A. Three dimensional photoacoustic imaging of blood vessels in tissue. Opt Lett 1998; 23: 648–650.
81. Kim C, Song KH, Gao F, Wang LV. Sentinel lymph nodes and lymphatic vessels: noninvasive dual-modality in vivo mapping by using indocyanine green in rats–volumetric spectroscopic photoacoustic imaging and planar fluorescence imaging. Radiology 2010; 255(2): 442–450.
82. Klibanov AL, Rasche PT, Hughes MS, Wojdyla JK, Galen KP, Wible JH Jr, Brandenburger GH. Detection of individual microbubbles of ultrasound contrast agents: imaging of free-floating and targeted bubbles. Invest Radiol 2004; 39(3): 187–195.
83. Zhang L, Xu J, Letson A, Roberts C, Xu R. Targeted delivery of multifunctional microbubbles for anti-VEGF therapy of age-related macular degeneration. ARVO 2010 Annual Meeting, Fort Lauderdale, FL, 2010.
84. Xu R, Xu J, Zuo T, Shen R, Huang T, Tweedle M. Drug-loaded biodegradable microspheres for image-guided combinatory epi-genetic therapy. J Biomed Opt 2011; 16: 020507.
85. Lanza GM, Wickline SA. Targeted ultrasonic contrast agents for molecular imaging and therapy. Curr Probl Cardiol 2003; 28(12): 625–653.
86. Schmitz G. Ultrasonic imaging of molecular targets. Basic Res Cardiol 2008; 103(2): 174–181.
87. Korpanty G, Carbon JG, Grayburn PA, Fleming JB, Brekken RA. Monitoring response to anticancer therapy by targeting microbubbles to tumor vasculature. Clin Cancer Res 2007; 13(1): 323–330.
88. Lee DJ, Lyshchik A, Huamani J, Hallahan DE, Fleischer AC. Relationship between retention of a vascular endothelial growth factor receptor 2 (VEGFR2)-targeted ultrasonographic contrast agent and the level of VEGFR2 expression in an in vivo breast cancer model. J Ultrasound Med 2008; 27(6): 855–866.
89. Johnson VG, Schlom J, Paterson AJ, Bennett J, Magnani JL, Colcher D. Analysis of a human tumor-associated glycoprotein (TAG-72) identified by monoclonal antibody B72.3. Cancer Res 1986; 46(2): 850–857.
90. Khattak SF, Chin KS, Bhatia SR, Roberts SC. Enhancing oxygen tension and cellular function in alginate cell encapsulation devices through the use of perfluorocarbons. Biotechnol Bioeng 2007; 96(1): 156–166.
91. Unger EC, Porter T, Culp W, Labell R, Matsunaga T, Zutshi R. Therapeutic applications of lipid-coated microbubbles. Adv Drug Deliv Rev 2004; 56(9): 1291–1314.
92. Kiessling F, Huppert J, Palmowski M. Functional and molecular ultrasound imaging: concepts and contrast agents. Curr Med Chem 2009; 16(5): 627–642.
93. Kawabata K-I, Sugita N, Yoshikawa H, Azuma T, Umemura S-I. Nanoparticles with multiple perfluorocarbons for controllable ultrasonically induced phase shifting. Jap J Appl Phys 2005; 44(6B): 4548–4552.
94. Kripfgans OD, Fowlkes JB, Miller DL, Eldevik OP, Carson PL. Acoustic droplet vaporization for therapeutic and diagnostic applications. Ultrasound Med Biol 2000; 26(7): 1177–1189.
95. Gao Z, Kennedy AM, Christensen DA, Rapoport NY. Drug-loaded nano/microbubbles for combining ultrasonography and targeted chemotherapy. Ultrasonics 2008; 48(4): 260–270.
96. Pisani E, Tsapis N, Paris J, Nicolas V, Cattel L, Fattal E. Polymeric nano/microcapsules of liquid perfluorocarbons for ultrasonic imaging: physical characterization. Langmuir 2006; 22(9): 4397–4402.
97. Huang J, Xu JS, Xu RX. Heat-sensitive microbubbles for intraoperative assessment of cancer ablation margins. Biomaterials 2010; 31(6): 1278–1286.
98. Xu RX, Povoski SP, Martin EW Jr. Targeted delivery of microbubbles and nanobubbles for image-guided thermal ablation therapy of tumors. Expert Rev Med Devices 2010; 7(3): 303-306.
99. Apfel R. Activatable infusable dispersions containing drops of a superheated liquid for methods of therapy and diagnosis. US Patent, 5,840,276, 1998.
100. Giesecke T, Hynynen K. Ultrasound-mediated cavitation thresholds of liquid perfluorocarbon droplets in vitro. Ultrasound Med Biol 2003; 29(9): 1359–1365.
101. VanSonnenberg E, McMullen EM, Solbiati L, Livraghi T, Mueller PR, Silverman SG. Tumor ablation: Principles and Practice. Springer Science + Business Media, New York, 2005.
102. Garrean S, Hering J, Saied A, Hoopes PJ, Helton WS, Ryan TP, Espat NJ. Ultrasound monitoring of a novel microwave ablation (MWA) device in porcine liver: lessons learned and phenomena observed on ablative effects near major intrahepatic vessels. J Gastrointest Surg 2009; 13(2): 334–340.
103. Topp SA, McClurken M, Lipson D, Upadhya GA, Ritter JH, Linehan D, Strasberg SM. Saline-linked surface radiofrequency ablation: factors affecting steam popping and depth of injury in the pig liver. Ann Surg 2004; 239(4): 518–527.

104. Cha CH, Lee FT Jr, Gurney JM, Markhardt BK, Warner TF, Kelcz F, Mahvi DM. CT versus sonography for monitoring radiofrequency ablation in a porcine liver. AJR Am J Roentgenol 2000; 175(3): 705–711.
105. Breen MS, Breen M, Butts K, Chen L, Saidel GM, Wilson DL. MRI-guided thermal ablation therapy: model and parameter estimates to predict cell death from MR thermometry images. Ann Biomed Eng 2007; 35(8): 1391–1403.
106. Dewey WC. Arrhenius relationships from the molecule and cell to the clinic. Int J Hyperthermia 1994; 10(4): 457–483.
107. Raspet R, Slaton W. Evaporation-condensation effects on resonant photoacoustics of volatile aerosols. J Atmos Ocean Technol 2003; 20(5): 685–695.
108. Arnott WP, Moosmuller H, Sheridan PJ, Ogren JA, Raspet R, Slaton WV, Hand JL, Kreidenweis SM, Collett JL Jr. Photoacoustic and filter-based ambient aerosol light absorption measurements: instrument comparisons and the role of relative humidity. J Geophys Res 108(D1): 4034, doi:4010.1029/2002JD002165 (2003).
109. Pramanik M, Wang LV. Thermoacoustic and photoacoustic sensing of temperature. J Biomed Opt 2009; 14(5): 054024.
110. Shah J, Park S, Aglyamov S, Larson T, Ma L, Sokolov K, Johnston K, Milner T, Emelianov SY. Photoacoustic imaging and temperature measurement for photothermal cancer therapy. J Biomed Opt 2008; 13(3): 034024.
111. Campbell RB. Tumor physiology and delivery of nanopharmaceuticals. Anticancer Agents Med Chem 2006; 6(6): 503–512.
112. Weissleder R, Kelly K, Sun EY, Shtatland T, Josephson L. Cell-specific targeting of nanoparticles by multivalent attachment of small molecules. Nat Biotechnol 2005; 23(11): 1418–1423.
113. Chappell JC, Price RJ. Targeted therapeutic applications of acoustically active microspheres in the microcirculation. Microcirculation 2006; 13(1): 57–70.

